HHS Public Access

Author manuscript

Plast Reconstr Surg. Author manuscript; available in PMC 2015 June 14.

Published in final edited form as:

Plast Reconstr Surg. 2014 November ; 134(5): 796e–805e. doi:10.1097/PRS.0000000000000696.

Electron Microscopic and Proteomic Comparison of Terminal Branches of the Trigeminal Nerve in Patients with and without Migraine Headaches

Bahman Guyuron, M.D., **Elizabeth Yohannes, Ph.D.**, **Robert Miller, Ph.D.**, **Harvey Chim, M.D.**, **Deborah Reed, M.D.**, and **Mark R. Chance, Ph.D.**

Departments of Plastic Surgery, Neurosciences, and Neurology, the Center for Proteomics and Bioinformatics, and the American Migraine Center, Case Western Reserve University

Abstract

Background—The purpose of this study was to compare the ultrastructural appearance and protein expression of the zygomaticotemporal branch of the trigeminal nerve in patients with and without migraine headaches.

Methods—After confirmation of migraine headache diagnosis on 15 patients, a 5-mm segment of the zygomaticotemporal branch of the trigeminal nerve that is routinely removed during migraine surgery was compared to similarly sized nerve segments obtained from 15 control patients without a history of migraine headaches, who underwent an endoscopic forehead lift where this nerve is routinely transected. The segments were snap-frozen at −80°C for the downstream proteomics analysis. In addition, the cytoarchitectural differences of the nerve segments obtained from the 15 migraine and 15 control subjects were examined in detail under the electron microscope.

Results—Analysis of liquid chromatography/tandem mass spectrometry data sets identified differentially expressed proteins and networks composed of highly connected molecular modules ($p = 10^{-44}$ and $p = 10^{-34}$) in patients with migraine headaches. The nerves from patients with migraine headaches had a linear organization, disrupted myelin sheaths and target axons, and discontinuous neurofilaments that were poorly registered with the discontinuous myelin sheaths, suggesting axonal abnormality.

Conclusions—This study offers electron microscopic and proteomic evidence of axonal abnormality and deregulation of the myelination process in patients with migraine headaches compared with controls, offering the first objective evidence to support the role of peripheral mechanisms in the migraine headache cascade and an explanation as to why the surgical treatment of migraine headaches is efficacious.

The pathophysiology of migraine headache is still incompletely understood. There are generally accepted mechanisms that play a role in the migraine cascade, including cortical

Bahman Guyuron, M.D., Department of Plastic Surgery, Case Western Reserve University, 29017 Cedar Road, Cleveland (Lyndhurst), Ohio 44124, bahman.guyuron@gmail.com.

Disclosure: The authors have no conflicts of interest to disclose.

hyperexcitability, dysfunctional periaqueductal gray matter, cortical spreading depression, and peripheral sensory nerve irritation.[1–3] As our understanding of migraine pathogenesis has progressed, particularly in relation to the small peripheral branches of the trigeminal and occipital nerves, interest in deactivation of these allodynic sensory nerves with botulinum toxin type A and targeted surgical therapy has evolved.[4–7]

Human and animal studies of compressed nerves have demonstrated various electron microscopic changes, including demyelination, axonal degeneration, changes in the perineurium and endoneural microvessels, the presence of Renaut bodies, connective tissue changes such as epineural and perineural fibrosis, and transient increases in Schwann cells.[8–10] The purpose of this study was to compare the ultrastructural appearance and protein expression of samples of the zygomaticotemporal branch of the trigeminal nerve in patients with and without migraine headaches to identify any abnormality that might potentially cause or contribute to triggering the headaches.

Patients and Methods

After securing institutional review board approval and confirmation by the research team neurologist that the 15 study patients had migraine headaches based on the International Classification of Headache Disorders II criteria,[11] 5-mm segments of the zygomaticotemporal branch of the trigeminal nerve (beyond the potential compression zone) that are routinely removed during migraine surgery (migraine group) were compared to similarly sized nerve segments obtained from 15 control patients without a history of migraine headaches (control group), who underwent standard endoscopic forehead lift, during which this nerve is routinely transected. The exact same harvest technique was used to obtain the nerve samples from both groups to eliminate the possibility that differences between groups could be attributed to artifact related to the nerve harvesting.

To compare the biochemical and molecular organization of peripheral nerve biopsy specimens from the control and migraine groups, longitudinal frozen sections were double-labeled with antibodies to neurofilament to detect axonal structure, and myelin basic protein to assess the organization of myelin sheaths. Excised nerves were immediately immersion fixed in 4% para-formaldehyde in 0.1 M phosphate buffer (pH 7.4) and stored at 4°C in fixative before sectioning. Longitudinal frozen sections were prepared using a Leica cryostat at −20°C and mounted on gelatin-coated slides. Before sectioning, nerves were immersed in 30% sucrose and embedded in optimal cutting temperature compound. Sections were air dried and stored at −20°C until use.

Sections were labeled with antibodies to myelin basic protein (SM 199; Convance, Princeton, N.J.) at 4°C overnight. Nonspecific staining was eliminated through condition of 5% bovine serum albumin into staining medium. To examine axonal localization and distribution, sections were labeled with a rabbit antineurofilament 68 kDa antibody (dilution, 1:2000; Chemicon International, Temecula, Calif.) overnight at 4°C. After incubation of primary antibodies, sections were labeled with appropriate secondary antibodies conjugated to Alexa Fluor 488 and 594 (Invitrogen, Carlsbad, Calif.). Sections were mounted in nonfade medium and examined on a light microscope equipped with fluorescence excitation.

Fluorescence and images were collected using a charge-coupled device camera at the same exposures. In addition, the cytoarchitectural differences in nerve segments obtained from the 15 migraine and 15 control subjects were examined in detail under the electron microscope.

For electron microscopy, peripheral nerve biopsy specimens were fixed in 4% paraformaldehyde and 2% glutaraldehyde in buffer for at least 48 hours at 4°C. Samples were then incubated in 1% osmium tetroxide for 1 to 3 hours, dehydrated through graded alcohols, and embedded in EPON 812 (Electron Microscopy Sciences, Hatfield, Penn.). One-micron-thick sections were cut using an ultramicrotome and stained with toluidine blue to identify areas of interest, and ultra-thin sections were then cut and stained with 1% uranyl acetate and 1% lead citrate. Sections were collected on polyvinyl Formvar–coated grids and examined using a Jeol 100 microscope (Jeol Ltd, Tokyo, Japan) at 80 kV.

Proteomic Evaluation

Nerve tissues obtained from the migraine and control groups were snap-frozen at −80°C for the downstream proteomics analysis. The typical sizes of extracted nerves were 5 mm and their wet weight was anywhere from 4.9 to 19.4 mg. Frozen nerve tissue samples ($n = 5$ per group for the original study and $n = 10$ per group for the follow-up study) were pulverized using a cryoPREP pulverizer (Covaris, Inc., Woburn, Mass.) and homogenized in lysis buffer (50 mM Tris-Hcl, pH 7.5, 4% sodium dodecyl sulfate, 40 mM dithiothreitol, and protease inhibitor cocktail). Lysates were reduced, alkylated, and fractionated using 1D sodium dodecyl sulfate polyacrylamide gel electrophoresis. Stained bands were cut horizontally into seven fractions, destained, and in-gel digested with trypsin. Once the digests were extracted into 60% acetonitriles and 0.1% formic acid, dried with SpeedVac (Thermo Fisher Scientific, Inc., Waltham, Mass.), and reconstituted in 0.1% formic acid, liquid chromatography/tandem mass spectrometry data were subsequently acquired for the individual fractions in the original study (70 liquid chromatography/mass spectrometry runs total).

In the follow-up study, the sample size per experimental group was much larger. To maintain consistent chromatographic reproducibility across the liquid chromatography/mass spectrometry runs, it was necessary to pool the proteolytic digests from each fraction into independent biological samples before acquiring liquid chromatography/tandem mass spectrometry data (20 liquid chromatography/mass spectrometry runs). Liquid chromatography/tandem mass spectrometry data for approximately 600 ng of each fraction in the initial study was acquired on an LTQ-FT mass spectrometer (Thermo Electron Corp., San Jose, Calif.) equipped with a Dionex Ultimate 3000 LC system (Dionex, Sunnyvale, Calif.). For the follow-up study, digests from gel fractions were precombined into biological replicate samples and liquid chromatography/tandem mass spectrometry data for the precombined aliquot containing 600 ng for each sample were acquired on an Orbitrap Velos Mass Spectrometer (Thermo Finnigan, Bremen, Germany) equipped with a Waters nanoACQUITY UPLC system (Waters, Inc., Milford, Mass.).

Data Analysis

Data Analysis Using the Elucidator—Retention time alignment, feature identification, and feature extraction across the entire chromatographic time window were performed using the PeakTeller algorithm in Rosetta Elucidator system v3.3 (Rosetta Biosoftware, Seattle, Wash.). For the initial study, fractions per biological replicate were precombined using a sum operation that stitches liquid chromatography/mass spectrometry data together. Chromatographic peak intensities belonging to the same precursor mass in the aligned chromatograms were squeezed to peptide and, similarly, intensity of peptides annotated to the same protein were added and subsequently used to calculate the relative peptide and protein abundance, respectively, on a section-by-section basis. In addition, expression ratios along with *p* values were computed by means of a multidimensional liquid chromatography ratio builder pipeline. The *p* values calculated are not from traditional analysis of variance, but instead are derived from an application of an error model developed for large-scale microarray data[12,13] as adapted for proteomics within the Elucidator program. For quality control, reproducibility of liquid chromatography/mass spectrometry chromatograms for all fractions was assessed for each group based on the retention time alignment and coefficients of variation. The relative retention time shifts to one master file to which all the files are compared were within ±2.4 minutes. Replicate reproducibility was also examined by calculating the coefficients of variation for all aligned and normalized features within each treatment group.

Database Search and Peak Annotation—The tandem mass spectrometry peak lists were extracted from tandem mass spectrometry data using Rosetta Elucidator. The resulting peak lists were then searched in a database of theoretical peptide spectra derived from sequences (86,392 entries) present in International Protein Index Human by running Mascot algorithm of Mascot version 2.2.1 (Matrix Science, London, United Kingdom). Mascot searches were performed with maximum peptide and fragment ion mass tolerance of 10 ppm and 0.8 Da, respectively, with variable methionine oxidation, and carbamidomethylation of cysteine, and one missed cleavage site was also allowed in the search parameters. The search results were imported back into Elucidator and concurrently validated with the PeptideTeller and ProteinTeller algorithms. The search result data were then filtered at 0.8 minimum probability and a predicted error of 0.02, and with these stringent criteria, 835 proteins (3368 peptides) were accepted as correctly identified for the initial study and 771 (4150 peptides) were identified for the follow-up study. The normalized peptide intensities annotated to the same protein were summed to gain a measure of the relative protein abundance between samples. To identify proteins whose expression levels are mediated by migraine, relative quantitation of all the identified proteins (835 in the initial and 771 proteins in the follow-up studies) was performed using a multidimensional liquid chromatography ratio builder pipeline within Elucidator. Proteins with changes 1.5-fold and above or −1.5-fold and below ($p < 0.05$) were considered as statistically significant taking into account the within-median coefficient of variation of approximately 40 percent.

Network Analysis—The data set with a list of regulated proteins identified by label-free liquid chromatography/tandem mass spectrometry was analyzed further using the network building tool Ingenuity Pathway Analysis (Ingenuity Systems, Inc., Redwood City, Calif.) to

understand the relationship of proteins and the effects of their abundant changes in the context of their cellular function, to identify potentially co-regulated partner proteins, and to ascertain their interactions with other known proteins. With this system biology tool, networks were generated using a data set of differentially expressed proteins. These proteins were overlaid onto a global molecular network developed from information contained in the Ingenuity Pathways Knowledge Base. Networks of these focus proteins were then algorithmically generated based on their connectivity. Subsequently, functional analysis of networks and/or the entire data set with significant differential expression was performed. A Fisher's exact test was used to calculate a *p* value determining the probability that each biological function and/or disease assigned to that pathway or network is attributable to chance alone.

Results

Electron Microscopy

Axonal and Myelin Changes in Peripheral Nerves of the Migraine Group—In control nerves, anti–myelin basic protein labeling revealed longitudinally oriented myelin sheaths that had a characteristic wavy appearance (Fig. 1, *above*). Low-magnification images revealed a relatively uniform distribution of myelinated axons throughout the nerve interspersed with unmyelinated regions. Double labeling with anti-neurofilament antibodies showed a tight register between the organization of the myelin sheaths and their axons. Neurofilaments appeared to be uniformly expressed along the length of the nerve and had a similar wavy appearance. Superimposition of the two images confirmed the intimate and complete registration of the axons with their surrounding myelin sheath. By contrast, comparable analysis of identically treated, similarly sized migraine-derived nerves revealed a more linear organization (Fig. 1, *center* and *below*). Labeling with antibodies to myelin basic protein revealed more clearly defined individual myelin sheaths, which labeled with high intensity, suggesting fewer myelinated axons in these nerves. A proportion of the myelin sheaths appeared discontinuous and nonuniform along their length. The pattern of neurofilament expression was strikingly different between migraine- and control-derived nerves. In migraine-derived nerves, the neurofilaments were discontinuous and poorly registered with the myelin sheaths. Rather than uniform longitudinal neurofilament expression, large regions of the nerve contained axons with patchy neurofilament interspersed with an apparent absence of neurofilaments, suggesting axonal abnormality. Not all nerves had the same level of axonal abnormality. For example, the images from migraine sample 1 (Fig. 1, *center*) show pronounced abnormality, whereas the images from migraine sample 2 have less abnormality. All migraine-derived nerves, however, had some level of axonal and myelin abnormality that was absent from controls. Although migraine nerves demonstrated axonal abnormality, there was no evidence for increased cellularity of the nerve and no obvious immune cell infiltration, even in pathologic regions.

Transverse sections through normal nerves revealed the characteristic arrangement of myelinated and unmyelinated axons (Fig. 2, *left*). In general, the myelinated axons were larger, and contained numerous mitochondria in microtubule-rich domains and little endoplasmic reticulum. The myelin sheaths were tightly apposed to the axolemma and there

was a characteristic 1:1 relationship between myelinating Schwann cells and their target axons. Unmyelinated axons were abundant, and individual unmyelinating Schwann cells were associated with multiple small-diameter axons. Individual Schwann cells were surrounded by a basement membrane, and there was extensive collagen and occasional interstitial fibroblasts distributed throughout the nerve. Longitudinal sections provided similar insights, with compact myelin associated with large-diameter axons. Some disruption of the organization of nodes of Ranvier and Schmidt-Lanterman clefts was apparent (Fig. 2, *right*), presumably as a consequence of the immersion fixation of the biopsy material.

Ultrastructural analysis provided additional insights into the pathologic disruption of the organization of migraine-derived nerves. The arrangement of a 1:1 association between a myelinating Schwann cell and its target axons was generally maintained (Fig. 3, *left*), although an occasional myelinating Schwann cell appeared to be associated with more than one axon. Throughout the nerves, however, the organization of a significant number of myelin sheaths and their target axons was disrupted. The most striking feature was the excessive amount of myelin surrounding the axon. Frequently, this myelin was folded and constricted the axon, leaving little axonal cytoplasm. The unmyelinated Schwann cell axon units were also affected (Fig. 3, *left* and *below*, *right*). In general, there were fewer unmyelinated axons associated with each Schwann cell, and the unmyelinated axons were less closely packed. Longitudinal images confirmed the disruption of the organization of myelinated axons (Fig. 3, *above*, *right*). In some cases, exuberant myelin was folded into loops that appeared to separate the axon into ovoids. In other cases, the axons appeared intact, but the myelin sheaths were thin and not closely associated with the target axon or completely absent.

Proteomics Analysis

Assessment of Reproducibility of Liquid Chromatography/Tandem Mass Spectrometry—

Although minor drifts in retention time are generally unavoidable, especially when larger sample numbers and replicates are analyzed as part of an extensive study, retention time shift was within a tolerable alignment search distance (±4 minutes) and, as a result, successful retention time alignment was attained using the Elucidator peak alignment algorithm. Coefficients of variation for the normalized intensities of approximately 835 proteins indicate good reproducibility and, for approximately 70 percent of the data set, were found at coefficients of variation of less than 35 percent for the control data and less than 40 percent for the migraine data, similar to previous studies.[14,15]

Differential Expressed Protein—

We report a total of 173 proteins in the initial assessment and 52 proteins in the follow-up assessment that have 1.5-fold and above or −1.5-fold and below changes in expression in the migraine subjects compared with the control subjects. It is not surprising to see a larger number of proteins identified in the initial study compared with the follow-up study, as the liquid chromatography/tandem mass spectrometry data in the initial study were acquired for each fractionated sample as opposed to pooled fractions in the follow-up study. In the two studies, a total of five proteins including MYH9, PRDX2, AHNAK, STOM, and PARK7 were common. In terms of

directionality of the fold changes, these proteins, except PARK7, were consistent between the two studies.

Networks of Proteins Mediated by Migraine Headaches—The pathway analysis on the data sets from the original study predicted the involvement of the top five significant pathways that are listed in Table 1. The ephrin-B signaling pathway was the most significant, and more than 16 percent of the molecules on this pathway were deregulated by migraine headaches. Therefore, the ephrin-B signaling pathway was deemed to be maximally deregulated in subjects with migraine headaches based on protein expression analysis. In addition, de novo network analysis provided the top two most significant networks of interactions, shown in Figure 4 (with values of $p = 10^{-44}$ and $p = 10^{-34}$, respectively).

Discussion

It is unclear whether the pathologic condition seen in the nerves of migraine sufferers is a consequence of a primary axonal deficit or whether it is the result of myelin disruption. Although a similar pathologic condition has been described in animals with disrupted myelin proteins (at least in the central nervous system),[16] several lines of evidence suggest this might be a primary axonal problem. There is a disruption in the organization of the unmyelinating Schwann cells, suggesting that it is not simply myelination. There are also organelle clusters in some axons where the myelin sheaths appear perfectly intact. Furthermore, there is clear sparing of some axons even in the worst conditions. The data suggest that there is a disruption in the interactions between axons and their target axons, reflecting the lack of a stable axon/Schwann cell unit.

The identified protein networks consist of highly interacting molecular modules displaying mainly synchronized differential expression in subjects with migraine. For instance, in the two networks shown in Figure 4, it is clearly delineated that molecular modules that are mainly involved in cytoskeletal organization are down-regulated as a function of disease. These included class IV intermediate filament proteins that are important in organization, assembly, and clustering of neurofilaments; and several tubulin isoforms, major components of the microtubule network. It has been demonstrated with transgenic and gene-targeted mice that neurofilaments are essential for the establishment of normal axonal calibers. Absence[17] or strong reduction[18,19] in axonal neurofilament numbers markedly suppresses the growth in axonal diameter that initiates during myelination. In addition to down-regulation of the different forms of neurofilaments and their interactors, proteins that are the structural constituent of myelin sheath and proteins that are involved in myelination of axons are also down-regulated in migraine subjects. This concurrent down-regulation of proteins that is very important for nervous system development and function in migraine subjects suggests a strong association between migraine and deregulation of the myelination process.

On both networks (Fig. 4), it is also clearly shown that the proteins that are up-regulated as a function of disease include a cluster of proteins that are involved in free radical scavenging. Peroxiredoxin 1 and 2 belong to a family of ubiquitous proteins that function as antioxidant cytoprotective proteins in all eukaryotic organisms. In general, they use electrons from

thioredoxin or other sulfhydryl donors to reduce cellular peroxides, including hydrogen peroxide.[20] Peroxiredoxins may participate in the signaling cascades of growth factors and tumor necrosis factor-α by regulating the intracellular concentration of hydrogen peroxide.[21] The up-regulation of peroxiredoxin 1 and 2 suggests that oxidative insult is part of the migraine disease process, and that they play a role in protecting proteins and lipids against oxidative damage.

It is also evident on the subnetwork (Fig. 4, *above*) that components of the actin cytoskeleton and cellular motor proteins (myosin) that are responsible for actin-based motility are up-regulated as a function of disease. Neuronal dynamics are powered by molecular motors such as microtubular or actin-based myosin. In migraine subjects, components of microtubular motors (Fig. 4, *below*) that are essential for neurogenesis and power the vesicular transport of building materials during neurite assembly are down-regulated. In contrast, components of actin-based motors that are responsible for cell motility, growth cone movement, and neurite outgrowth are up-regulated, suggesting enhanced molecular motor rearrangement with migraine.[22]

We were also able to predict the expression status of upstream transcriptional regulators using a recently incorporated mechanistic network algorithm within Ingenuity Pathway Analysis. The predicted activation of transcriptional factors including SRF and MYOCD but deactivation of RUNX2 could be responsible for the overexpression of the different forms of myosin, vinculin, and tropomyosin in migraine patients.

Overall, the interactions described by these top-scoring networks provide a framework for evaluating our targets and enable us to identify the involvement of new functional complexes such as nuclear factor-κB and NFAT and upstream transcriptional factors that are possibly deregulated in subjects with migraine.

Conclusions

The role of peripheral mechanisms in triggering migraine headaches has become increasingly prominent.[3,23] This is evidenced by elimination or reduction of migraine headaches with the injection of botulinum toxin type A or peripheral nerve surgery. Findings from the current study further support the role of peripheral mechanisms in triggering migraine headaches and offer an explanation as to why the surgical treatment of migraine headaches is effective. These findings may also lead to other opportunities to treat patients with migraine headaches noninvasively, or with less invasive procedures that repair the defective myelin around nerves, lending additional protection to the nerves.

Acknowledgments

This work was funded by a grant from the Prentiss Foundation.

References

1. Bernstein C, Burstein R. Sensitization of the trigeminovascular pathway: Perspective and implications to migraine pathophysiology. J Clin Neurol. 2012; 8:89–99. [PubMed: 22787491]

2. Edvinsson L, Villalón CM, MaassenVanDenBrink A. Basic mechanisms of migraine and its acute treatment. Pharmacol Ther. 2012; 136:319–333. [PubMed: 22939884]
3. Vecchia D, Pietrobon D. Migraine: A disorder of brain excitatory-inhibitory balance? Trends Neurosci. 2012; 35:507–520. [PubMed: 22633369]
4. Guyuron B, Tucker T, Davis J. Surgical treatment of migraine headaches. Plast Reconstr Surg. 2002; 109:2183–2189. [PubMed: 12045534]
5. Guyuron B, Kriegler JS, Davis J, Amini SB. Comprehensive surgical treatment of migraine headaches. Plast Reconstr Surg. 2005; 115:1–9. [PubMed: 15622223]
6. Guyuron B, Kriegler JS, Davis J, Amini SB. Five-year outcome of surgical treatment of migraine headaches. Plast Reconstr Surg. 2011; 127:603–608. [PubMed: 20966820]
7. Guyuron B, Reed D, Kriegler JS, Davis J, Pashmini N, Amini S. A placebo-controlled surgical trial of the treatment of migraine headaches. Plast Reconstr Surg. 2009; 124:461–468. [PubMed: 19644260]
8. Gupta R, Steward O. Chronic nerve compression induces concurrent apoptosis and proliferation of Schwann cells. J Comp Neurol. 2003; 461:174–186. [PubMed: 12724836]
9. Kobayashi S. Localization and changes of intraneural inflammatory cytokines and inducible-nitric oxide induced by mechanical compression. J Orthop Res. 2005; 23:771–778. [PubMed: 16022989]
10. Myers RR. Anatomy and microanatomy of peripheral nerve. Neurosurg Clin N Am. 1991; 2:1–20. [PubMed: 1668260]
11. Headache Classification Subcommittee of the International Headache Society. The International Classification of Headache Disorders: 2nd edition. Cephalalgia. 2004; 24(Suppl 1):9–160. [PubMed: 14979299]
12. Dai H, Meyer M, Stepaniants S, Ziman M, Stoughton R. Use of hybridization kinetics for differentiating specific from non-specific binding to oligonucleotide microarrays. Nucleic Acids Res. 2002; 30:e86. [PubMed: 12177314]
13. Weng L, Dai H, Zhan Y, He Y, Stepaniants SB, Bassett DE. Rosetta error model for gene expression analysis. Bioinformatics. 2006; 22:1111–1121. [PubMed: 16522673]
14. Neubert H, Bonnert TP, Rumpel K, Hunt BT, Henle ES, James IT. Label-free detection of differential protein expression by LC/MALDI mass spectrometry. J Proteome Res. 2008; 7:2270–2279. [PubMed: 18412385]
15. Schlatzer DM, Dazard JE, Ewing RM, et al. Human biomarker discovery and predictive models for disease progression for idiopathic pneumonia syndrome following allogeneic stem cell transplantation. Mol Cell Proteomics. 2012; 11:M111–015479. [PubMed: 22337588]
16. Griffths I, Klugmann M, Anderson T, et al. Axonal swellings and degeneration in mice lacking the major proteolipid of myelin. Science. 1998; 280:1610–1613. [PubMed: 9616125]
17. Zhu Q, Couillard-Després S, Julien JP. Delayed maturation of regenerating myelinated axons in mice lacking neurofilaments. Exp Neurol. 1997; 148:299–316. [PubMed: 9398473]
18. Eyer J, Peterson A. Neurofilament-deficient axons and perikaryal aggregates in viable transgenic mice expressing a neurofilament-beta-galactosidase fusion protein. Neuron. 1994; 12:389–405. [PubMed: 8110465]
19. Elder GA, Friedrich VL Jr, Bosco P, et al. Absence of the midsized neurofilament subunit decreases axonal calibers, levels of light neurofilament (NF-L), and neurofilament content. J Cell Biol. 1998; 141:727–739. [PubMed: 9566972]
20. Simzar S, Ellyin R, Shau H, Sarafan TA. Contrasting antioxidant and cytotoxic effects of peroxiredoxin I and II in PC12 and NIH3T3 cells. Neurochem Res. 2000; 25:1613–1621. [PubMed: 11152390]
21. Gioio AE, Lavina ZS, Jurkovicova D, et al. Nerve terminals of squid photoreceptor neurons contain a heterogeneous population of mRNAs and translate a transfected reporter mRNA. Eur J Neurosci. 2004; 20:865–872. [PubMed: 15305855]
22. Even-Ram S, Doyle AD, Conti MA, Matsumoto K, Adelstein RS, Yamada KM. Myosin IIA regulates cell motility and actomyosin-microtubule crosstalk. Nat Cell Biol. 2007; 9:299–309. [PubMed: 17310241]
23. Malick A, Burstein R. Peripheral and central sensitization during migraine. Funct Neurol. 2000; 15(Suppl 3):28–35. [PubMed: 11200798]

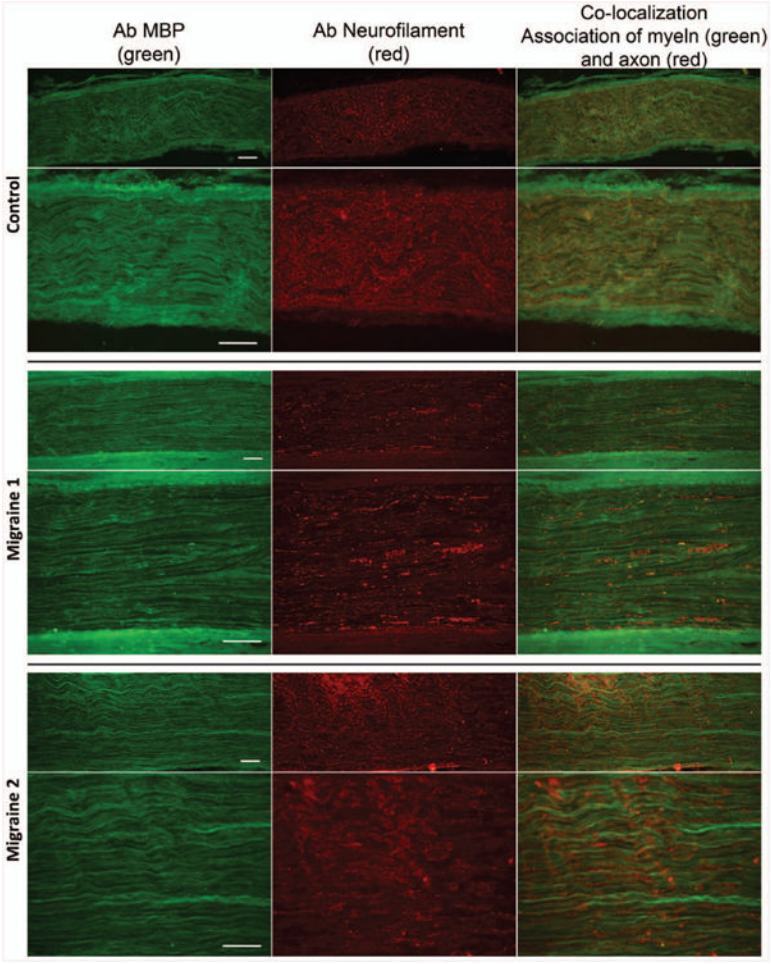

Fig. 1.

Comparison of the organization of myelin sheaths and axons in control- and migraine-derived nerves. (*Above*) Longitudinal sections through control-derived nerves. Low-magnification images labeled with antibodies to myelin basic protein (*MBP*) (*above*, *left*), neurofilaments (*above*, *center*), and the merged image (*above*, *right*). Myelin sheaths and their associated axons are uniformly distributed throughout the nerve, and the nerve demonstrates a characteristic wavy organization. (*Center*) Higher magnification images showing the close juxtaposition of myelin sheaths labeled with myelin basic protein (*center*, *left*) and their axons labeled with neurofilament (*center*, *center*). (*Center*, *right*) Merged image. (*Center*) Longitudinal sections through a migraine-derived nerve labeled with antibodies to myelin basic protein (*above*, *left* and *center*, *left*), neurofilaments (*above*, *center* and *center*, *center*), and the merged image (*above*, *right* and *center*, *right*). Note that in contrast to control nerves, the nerve has a less wavy appearance, the myelin sheaths are more pronounced, and the neurofilament labeling is discontinuous along the length of the axon. Regions of intense neurofilament staining are interspersed with a lack of neurofilament staining. (*Below*) An additional example of a migraine-derived nerve showing the disorganization of myelin sheaths, the lack of continuity of neurofilament expression, and the lack of tight correlation between myelin basic protein labeling and neurofilaments.

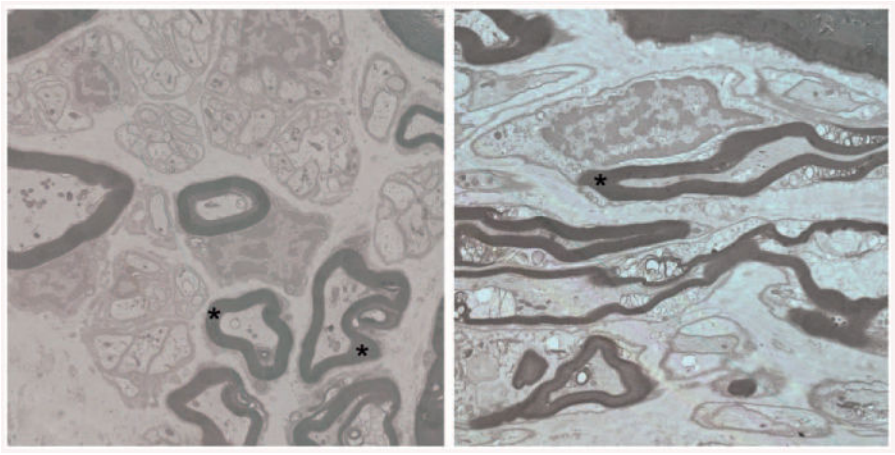

Fig. 2.

(*Left*) Transverse section through control-derived nerves showing characteristic organization of myelinated and unmyelinated axons. Myelinated axons are relatively larger and surrounded by intact myelin (*) that is closely apposed to the axolemma. Axons contain numerous mitochondria and vesicles in distinct axonal domains. The characteristic 1:1 association of Schwann cells and myelinated axons is evident. The nerve also contains numerous unmyelinating Schwann cells that are associated with multiple small-diameter axons. Each Schwann cell is surrounded by a basal lamina. (*Right*) Longitudinal section through control nerves showing the close juxtaposition of axon and myelin sheaths (*). Some disruption of myelin organization is apparent at nodes of Ranvier and Schmidt-Lanterman clefts, presumably as a consequence of immersion fixation.

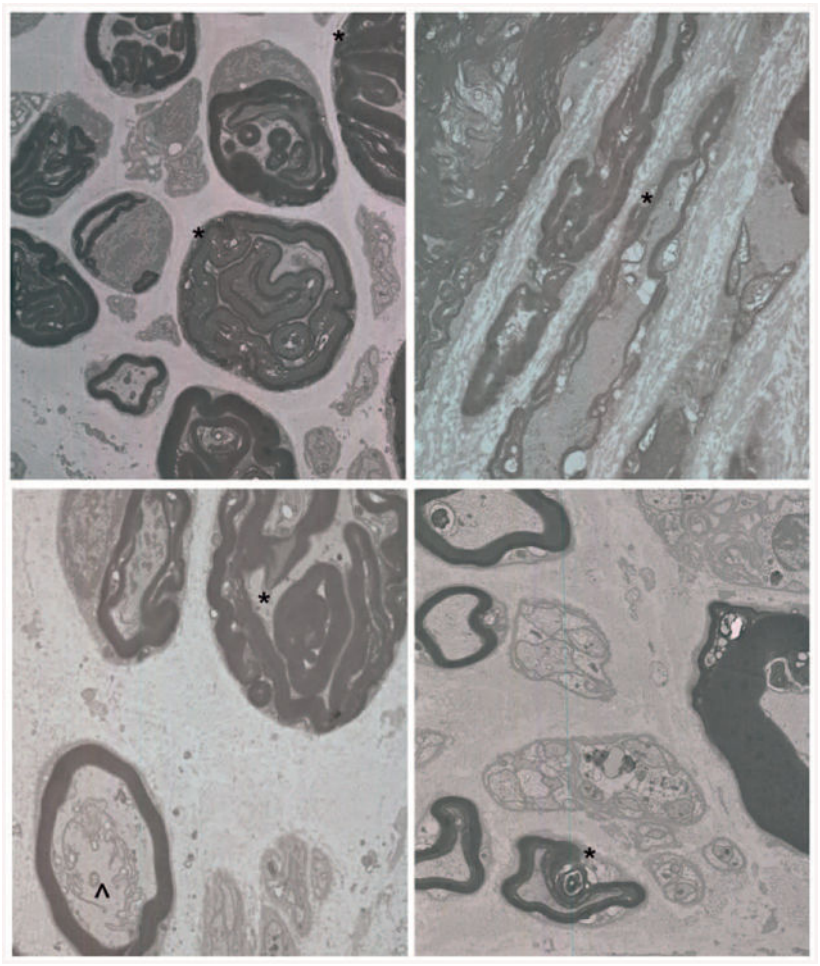

Fig. 3.

Sections through migraine-derived nerves demonstrate perturbations in axon/Schwann cell interactions. (*Above*, *left*) Transverse section through migraine-derived nerve shows the maintenance of the 1:1 relationship between Schwann cells and myelinated axons. Although some myelinated axons have a normal cytoarchitecture, many axons appear to be shrunken and surrounded and encased by multiple layers of myelin (*). Unmyelinating Schwann cells appear to be associated with fewer than normal axons. Each Schwann cell is surrounded by a basal lamina and collagen. (*Above*, *right*) Longitudinal section demonstrating perturbation of myelin and axon organization. Although some axons appear intact, the myelin sheaths are thin, absent, or overlapping (*). (*Below*, *left*) Transverse section through another example showing tongues of myelin interceding and constricting the axon (*), whereas in a normal appearing myelinated axon there is a collection of rough endoplasmic reticulum and other membranous organelles that are not organized in distinct domains (^). (*Below*, *right*) Dysmyelinated axons also show architectural disruption, including lack of tight juxtaposition between Schwann cell and axon and some axonal loss (*). Not all axons are equally affected, although perturbation abnormality affected large-and small-diameter axons equally.

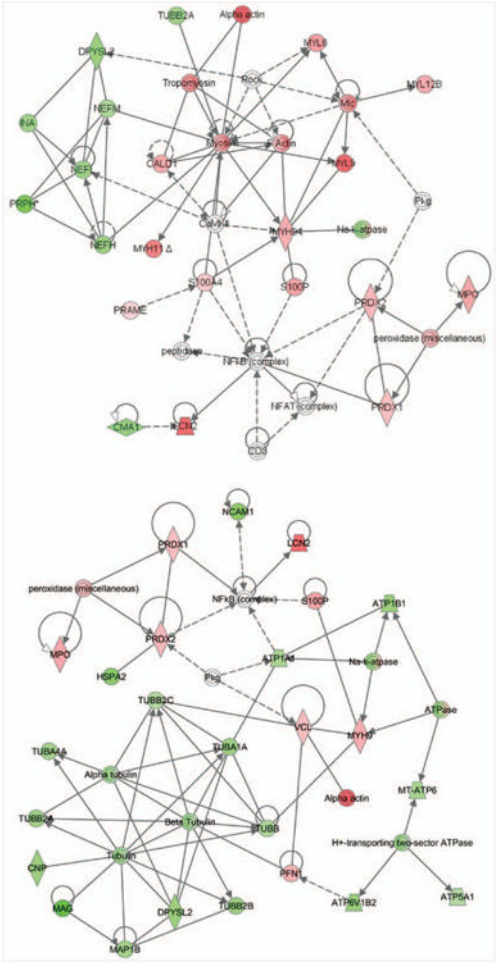

Fig. 4.

Networks of proteins associated with migraine were generated using Ingenuity Pathway Analysis tools. These networks are the most significant and neurologic disorder enriched networks. On these networks, nodes (proteins) with the *red* and *green* highlights are identified as up- and down-regulated, respectively, in migraine subject compared with controls. Individual proteins are represented as *nodes*, and the different shapes of the nodes represent the functional class of the proteins. The *edges* define the relationships of the nodes; the *arrowheads* indicate the direction of the interaction.

Table 1

Cellular Pathways with Greater-Than-Chance Representation by Signature Proteins

Pathways	Expectation	Saturation Ratio (%)
Ephrin-B signaling	2.95E-11	16.2
RhoGDI signaling	3.67E-09	8.1
Axonal guidance signaling	1.12E-08	5.2
Germ cell–Sertoli cell junction signaling	4.28E-08	8.5
Signaling by Rho family GTPases	1.46E-07	6.3